
PARADOXICAL IMPACT OF SPRAWLING INTRA-URBAN HEAT ISLETS: REDUCING MEAN SURFACE TEMPERATURES WHILE ENHANCING LOCAL EXTREMES

A PREPRINT

**Anamika Shreevastava^{1,*}, Saiprasanth Bhalachandran^{2,+}, Gavan S. McGrath³,
Matthew Huber², and P. Suresh C. Rao¹**

1. Lyles School of Civil Engineering, Purdue University, West Lafayette, IN, USA

2. Department of Earth, Atmospheric, and Planetary Sciences, Purdue University, IN, USA

3. Ecosystem Science, Department of Biodiversity Conservation and Attractions, Kensington, WA, Australia

+Current affiliation: Department of Earth System Science, Stanford University, CA, USA

*Corresponding author: ashreeva@purdue.edu; <http://anamika255.github.io>

ABSTRACT

1 Cities are at the forefront of climate change impacts and face a growing burden of adaptation to
2 ensuing natural hazards. Extreme heat is a particularly challenging hazard as persistent heatwaves
3 are locally exacerbated by the Urban Heat Island (UHI) effect. As a result, there is an increasing sci-
4 entific interest in the influence of diverse urban morphologies on UHI. However, as the temperatures
5 within cities are highly spatially heterogeneous, bulk quantification metrics such as UHI Intensity
6 may hamper understanding. Here, we use remotely sensed Land Surface Temperature (LST) data
7 for 78 diverse cities to develop a novel multi-scale framework of quantifying spatial heterogene-
8 ity in the Surface UHI. We identify heat clusters emerging within the SUHI using percentile-based
9 thermal thresholds and refer to them collectively as *intra-Urban Heat Islets*. We first develop a La-
10 cunarity based metric (Λ_{score}) to quantify the spatial organization of heat islets at various degrees
11 of sprawl and densification. Using probabilistic models, we condense the size, spacing, and inten-
12 sity information about heterogeneous clusters into distributions that can be described using single
13 scaling exponents. This allows for a seamless comparison of the heat islet characteristics across
14 cities at varying spatial scales. From the size distribution analysis, we observe the emergence of two
15 distinct classes wherein the dense cities (positive Λ_{score}) follow a Pareto size distribution, whereas
16 the sprawling cities (negative Λ_{score}) show an exponential tempering of Pareto tail. This indicates a
17 significantly reduced probability of encountering large heat islets for sprawling cities. Contrastingly,
18 however, Heat Islet Intensity modeled as exponential distributions reveal that a sprawling configu-
19 ration is favorable for reducing the mean temperature of a city. However, for the same mean SUHI
20 intensity, it also results in higher local thermal extremes. This poses a paradox for urban designers
21 in adopting expansion versus densification as a growth trajectory to mitigate the UHI.

22 Introduction

23 More than 50% of the world’s population currently resides in cities, and the number continues to increase rapidly with a
24 projection that 70% of the global population will be urbanized by 2050 (Prudhomme, 2018). Rapid urbanization trends
25 are manifested in expansion and densification of existing cities and the merging of agglomerations to form megacities,
26 particularly in South Asia and sub-Saharan Africa (Seto and Shepherd, 2009). Among the numerous challenges that
27 cities face, a particularly urgent problem due to climate change is that of extreme heat. Urban areas often raise the
28 local temperatures relative to natural and rural surroundings leading to the phenomenon of Urban Heat Island (UHI)
29 effect. A synergistic interaction between UHIs and increasingly persistent heat waves further exacerbates the extreme
30 temperatures within cities (Li and Bou-Zeid, 2013; Zhao et al., 2018). Repercussions of extreme heat include thermal
31 discomfort (Nikolopoulou and Lykoudis, 2006), increased energy consumption (Santamouris, 2014), and a greater
32 number of heat-related casualties during heat waves (Semenza et al., 1996; Uejio et al., 2011).

33 The UHI is typically quantified as UHI Intensity, i.e. the difference between the air temperatures of a represen-
34 tative urban area (point measurement or spatial average) and rural area. However, such an estimate is inadequate to
35 address the *intra-urban* spatial heterogeneity. Commendable efforts to collect spatially resolved thermal data such as
36 the Basel Urban Boundary Layer Experiment (BUBBLE) campaign (Rotach et al., 2005) are rare and often limited to
37 a single city. On the other hand, earth-monitoring satellites such as Landsat and Moderate Resolution Imaging Spec-
38 troradiometer (MODIS) enable consistent high spatial resolution characterization across multiple cities. As a result,
39 the Surface UHI (SUHI) estimated using Land Surface Temperatures (LST) has emerged as an alternative approach
40 which we adopt in this study (Roth et al., 1989; Voogt and Oke, 2003). For satellite sensors, urban features such as
41 building roof and wall exteriors, surface materials, albedo, impervious and vegetated fractions, and surface moisture
42 within each pixel determine the resultant LST. Note that while SUHI bears similarity in spatial and temporal patterns
43 to UHI, spatial patterns of SUHI are more coupled with urban form and function, whereas air temperatures are subject
44 to the boundary layer wind profiles as well, therefore, a point-to-point correspondence can not be expected (Panwar
45 et al., 2019).

46 LST, which is strongly determined by the land use land cover properties, emerges from the underlying self-
47 organization of the urban forms. As a result, the role of spatial organization of urban form in reducing SUHI Intensity
48 has been a topic of substantial research spanning multitude of spatial scales. At the micro-scale, i.e. within the urban
49 canyon, the surface temperatures are extremely sensitive to the geometrical details of immediate surroundings, such
50 as street canyon geometry, sky-view factor, vegetative fraction, solar access and shading (Jamei et al., 2016; Taleghani
51 et al., 2015; Andreou, 2013). However, at the local scale, i.e. of the order of few kilometers, consistent thermal patterns
52 emerge due to locally homogeneous patches of urban form and function (Stewart and Oke, 2012; Ching et al., 2018).
53 We do not have a clear understanding of the optimal urban form and function that minimize the urban heat locally
54 as well as at a city-scale. For instance, studies investigating local scale impacts (Sobstyl et al., 2018; Schwarz and
55 Manceur, 2014) report that high-density urban development leads to higher local temperatures, whereas, several others
56 note that sprawling urban development may result in worse thermal conditions (Stone Jr and Rodgers, 2001; Stone
57 et al., 2010). Debbage and Shepherd (2015) (Debbage and Shepherd, 2015) show that regardless of the urban density
58 type *within a patch*, the relative spatial contiguity of the urban land use patches is a critical variable as well. Despite
59 these recent advances on the intra-urban thermal landscape over the last few decades, a comprehensive framework for
60 the characterization of intra-urban thermal heterogeneity for diverse city morphologies is still lacking.

61 We use a multi-scale framework wherein we treat the SUHI not as a single entity, but as a collection of heterogeneous
62 clusters of heat within the city. We refer to these clusters as **intra-urban heat islets**. The objective of this study is
63 to evaluate the impact of spatial organization of these heat islets on their properties such as size and intensity and

determine if there is a favourable spatial structure for reducing surface temperature extremes at intra-urban spatial scales. Urban morphology, and as a result LST, emerges via the processes of densification and expansion, albeit constrained by cultural, geographic and economic factors (Batty, 2013; Mustafa et al., 2018). Different degrees and combinations of these two processes result in diversity of form and function. Dense urban growth occurs when there is increased in-fill construction within existing high-density built-up area. Such a process is often driven by economic and socio-political factors that lead to settlement of new urban regions close to the city center (Andersson et al., 2006). This is akin to the preferential attachment phenomenon observed in complex networks where a new node is more likely to agglomerate at the "hub nodes" with the highest density of edges (Barabási and Albert, 1999). We hypothesize that the densification within urban area results in hot regions getting hotter and larger thereby resulting in a heavy-tailed size distribution of heat islets. Urban expansion in the form of sprawl, on the other hand, occurs at the periphery of urban areas in the form of growing sub-urban regions. We hypothesize that this would lead to the emergence of heat islets that are spread more evenly throughout the city, often interspersed with local heat sinks. This can be detected in the size distribution as a fast decaying tail, often in the form of an exponential tempering (Amaral et al., 2000). Similar effects of urban expansion and densification on the power-law node degree observed is observed in several urban infrastructure systems such as roads and sewage networks (Mohajeri et al., 2015; Yang et al., 2017; Klinkhamer et al., 2017). Note that we don't refer to the spatial organization of urban assets such as buildings or impervious areas. Rather, we directly analyze the LST. We implement the framework for a set of 78 cities sampled globally. Using probabilistic models, we condense the size, spacing, and intensity information about heterogeneous clusters into distributions that can be described using single scaling exponents. This allows for a seamless comparison of the heat islet characteristics across cities that represent varying degrees of sprawl or densification. We then assess how the thermal spatial structure relates to the traditional lumped metric, SUHI Intensity. Lastly, we discuss implications for desirable thermal configurations for cities to minimize the area and intensity of the heat islets.

Data acquisition and Clustering technique

A set of 78 cities were sampled encompassing diverse climatological, geographical, and cultural backgrounds as well as different realizations of urban form and function (Figure 1). The cities selected range from megalopolises such as Guangzhou, London, and New York City with a population of over 10 Million and metropolitan areas up to 3000 km², to smaller cities such as Tbilisi, Bern, and Oslo that span less than 100 km². As a globally standardized dataset of urban extent, the Urban Land Use layer of Land Cover product from MODIS was used. The exact definition of urban boundaries and city area plays a significant role in urban scaling laws (Cottineau et al., 2017), therefore, a buffer of 5 km in the rural regions was taken to account for the peri-urban settlements. However, as the heat islets occur well within the city boundaries, the results were found to be independent of the buffer width.

For each city, we selected a Landsat image of a summertime cloud-free day, and derived the LST in the geospatial computing environment of Google Earth Engine (Gorelick et al., 2017) using the methodology described in Walawender et al. (2012) (Walawender et al., 2012). A novel aspect of our methodology is the clustering technique used to characterize the LST. The LSTs are treated analogously to topography in Digital Elevation Models (DEM), where the temperatures substitute for elevation (Shreevastava et al., 2018). As the cities belong to diverse climatic backgrounds (and hence, background temperatures) (Zhao et al., 2014), percentile-based thermal thresholds were chosen for identifying the relative hottest regions within the urban areas. The areas above a given thermal threshold (e.g., corresponding to percentiles of temperatures) were identified, and the connected pixels were grouped into a cluster that we refer to as a **heat islet**. Supplementary Information provides code and text describing the methods in more detail.

104 Size distribution of heat islets

105 In an exploration of *shapes* of heat islets, we found consistent self-similar, fractal topography across all cities (Shreev-
 106 astava et al., 2019) (See Supplementary Figure 1). Here, we focus on their *size* distribution by building on the scaling
 107 laws known for fractal surfaces. According to Korcak’s law, the size distribution of clusters in a fractal topography is
 108 expected to follow a power law at the percolation threshold (Imre and Novotný, 2016; Mandelbrot, 1975; Isichenko
 109 and Kalda, 1991). This is mathematically represented as: $N(a) \propto a^{-\beta}$ where N is the number of clusters of area, a ,
 110 and the scaling exponent is β . Expressed as an exceedance probability we can write it as a Pareto distribution:

$$P(A \geq a) \propto a^{1-\beta}, \quad \forall a \geq a_{min} \quad (1)$$

111 where, for a given area a , the probability of an islet having an area A larger than a is represented by P , the scaling
 112 exponent is represented by β , and the minimum area at or above which the power-law is valid is represented as a_{min} .
 113 We use Maximum Likelihood Estimation (MLE) to test for and fit the exceedance probability distributions (Clauset
 114 et al., 2009) (See Supplementary Text 3). This process is carried out for multiple thermal thresholds (50th, 60th, \dots ,
 115 90th percentiles). We find that the estimated exponents ranged between 1.6 to 2.2 with a mean $\beta = 1.88$. However,
 116 for the smaller cities ($A_{city} \leq 650 \text{ km}^2$), the variability in exponents was much larger (Supplementary Figure 2).
 117 One explanation for this is statistical, wherein for small cities there are not enough islets obtained at 90 m resolution
 118 which results higher statistical fluctuations about the mean are observed. As the number of islets increases with city
 119 size, steady averaging is achieved that results in convergence towards the mean. However, from an urban growth
 120 perspective, this behavior is consistent with several other complex systems that operate within cities (Klinkhamer
 121 et al., 2017; Barthelemy, 2016). For smaller cities, the variability due to factors unrelated to city size result in more
 122 detectable fluctuations and it simply indicates that they have not grown in size enough to display self-organization yet
 123 (Batty, 2008). We, therefore, excluded those from any further analysis and proceed with 49 cities where the internal
 124 thermal structure could be reliably quantified. For the larger cities, the distributions were well described by Equation
 125 1 with the same mean exponent and a narrow variability (std. dev. = 0.026) (Shreevastava et al., 2019).

126 The impact of a dense or sprawling spatial organization becomes apparent in how the exceedance probability dis-
 127 tributions change as the threshold increases. The large metropolitan regions of Lagos and Jakarta are selected as
 128 representatives of dense cities, where Chicago and Guangzhou are chosen to represent sprawling cities (Figure 2a,b).
 129 The Pareto size distribution is consistent at lower thresholds for all cities. At 90th percentile threshold, however, Lagos
 130 and Jakarta show a pronounced aggregation of heat islets indicative of dominance of a dense urban center, whereas
 131 Chicago and Guangzhou are more dispersed (Figure 2c,d). In agreement with our initial hypothesis, Lagos and Jakarta,
 132 display a Pareto heat islet size distribution across all the thresholds (Figure 2e). However, for Chicago and Guangzhou,
 133 the heat islet size distributions deviate significantly from the Pareto in the form of an exponential tempering (Figure
 134 2f), such that their distributions more closely follow:

$$P(A \geq a) \propto a^{1-\beta} \cdot e^{-c \cdot a}, \quad \forall a \geq a_{min} \quad (2)$$

135 where c represents the exponential tempering coefficient (Supplementary Table 3).

136 Such behavior is explained by invoking percolation theory (Isichenko, 1992; Sahimi and Sahimi, 2014). Percolation
 137 theory is the study of random clusters and their spatial connectivity at a given threshold. The coagulation of dispersed
 138 clusters into a contiguous component is referred to as percolation, and the largest cluster is identified as the percolating
 139 cluster. In fractal landscapes, the Pareto size distribution of clusters holds within a finite range (Percolation Transition
 140 Range) of thresholds, i.e., until the percolating cluster retains its identity. We computed the percolation transition range

141 by identifying the inflection points in the size of the largest cluster as a function of temperature threshold (Figure 2g,h).
 142 The range was then normalized using the minimum and maximum temperatures for each city such that the range is
 143 restricted to 0 and 1. We refer to this as the Normalized Percolation Range (NPR) (Supplementary Figure 3). In case
 144 of the aggregated cities (e.g. Jakarta and Lagos) as the temperature threshold is increased, the largest connected islet
 145 decreases in size gradually, and the resulting NPR is large (Figure 2g). Conversely, in the case of sprawling cities
 146 (e.g., Chicago and Guangzhou) there is a much sharper decrease in the size of the percolating cluster (Figure 2h)
 147 resulting in a narrow NPR (Figure 2i,j). As the 90th percentile thresholds in these cases fall outside the NPR (Figure
 148 2j), exponential tempering is observed.

149 From the perspective of the size distribution of heat islets alone, as the thermal threshold is increased, fewer and
 150 smaller heat islets are captured. Therefore, an exponential tempering presents a reduced probability of encountering
 151 large heat islets of higher temperatures. This suggests that a sprawling spatial structure is favourable for reducing
 152 the size of extreme heat islets. Thus far, we have characterized the size distribution of these islets, not their spatial
 153 organization. We now introduce a metric to quantify and analyze the relationship between the spacing of the urban
 154 heat islets and the characteristics we observed in their size distributions.

155 **Quantifying Aggregated vs Dispersed heat islets: Lacunarity**

156 A built-up patch in a city acts as a source of increased sensible heat flux, as well as anthropogenic heat flux due to
 157 human activities such as air-conditioning. Likewise, the gaps between the patches (also referred to as spacing in this
 158 work), often water or vegetation, act as heat sinks that absorb the excess heat generated. Therefore, characterizing this
 159 spacing between the urban patches is an essential step towards ameliorating heat stress (Debbage and Shepherd, 2015).
 160 Particularly, the impact of the relative sizes and strengths of such sources and sinks on the overall thermal landscape
 161 has been relatively understudied and requires further investigation. Since the present study focuses on the thermal
 162 landscape characterized by LST, we can directly quantify the spacing between the identified heat islets. Popular
 163 metrics such as root mean square distances work well for Gaussian systems, but for fractal landscapes, lacunarity is
 164 a better-suited metric of spatial structure (Plotnick et al., 1996). Lacunarity (Λ) is a scale-dependent measure of the
 165 aggregation of spaces between the heat islets (Mandelbrot, 1982; Plotnick et al., 1996). A ‘gliding box’ algorithm for
 166 the calculation of Λ as a function of box size (r), as described in Plotnick et al. (1993), was adopted here (Methods
 167 section). While the absolute values of Λ offer little insight, the appropriate way to interpret lacunarity is in the context
 168 of the rate of change of Λ as a function of r . If the value of $\log(\Lambda(r))$ decreases at any scale (quantified with $\log(r)$),
 169 the presence of spacing corresponding to that length scale is indicated. The two extremes of lacunarity curvature can
 170 be best conceptualized as a chessboard-type homogeneous distribution of small-scale spacing, and a single contiguous
 171 cluster. Essentially, the length scales corresponding the steepest slopes should be interpreted as the dominant scale of
 172 spacing.

173 As the differences in the spatial organization of heat islets are most apparent at higher temperature thresholds, here,
 174 we characterized the spatial structure obtained at the 90th percentile of LST for all cities. By extension, the total
 175 *islet area* under consideration corresponds to the hottest 10% of the total city area. Lacunarity curves for the four
 176 representative cities investigated in the previous section are highlighted in Figure 3. The cities that have a dominance
 177 of larger spacing between the islets lay above the diagonal. Conversely, a dispersed spatial structure of the heat islets
 178 manifests as smaller spacing, fall under the diagonal. We assign a single score (Λ_{score}) to the convexity of the curves

179 in Figure 3a such that positive scores indicate larger spacing and vice-versa. This is achieved using the following
 180 empirical equation:

$$\log_{10}(\Lambda(r)) = \left(1 - \frac{\log_{10}(r)}{2}\right)^{2^{\Lambda_{score}}} \quad (3)$$

181 where constants 1 and 2 are used to fix the end points of the curve at $\log(\Lambda(r)) = 1$ and $\log(r) = 2$, and the exponent,
 182 Λ_{score} is scale-independent measure of the shape of the lacunarity curve (See Methods section). The 49 cities have
 183 Λ_{score} ranging between -0.9 to 0.6, and distributed normally (Figure 3b; See Supplementary Table 4).

184 Using Λ_{score} , we compare the relationship between the islet spacing and their NPR (and by extension, likely expo-
 185 nential tempering at higher thresholds). We find that the dense cities associated with an aggregated heat islet structure
 186 (positive Λ_{score}) display a larger NPR (≥ 0.25 ; Figure 3c). Whereas, sprawling and disaggregated cities (negative
 187 Λ_{score}) have a smaller NPR (< 0.25 ; Figure 3c) and consequently an exponential tempering of the power law tail
 188 (Figure 2f). An exception to this pattern are cities with a negative Λ_{score} despite having an NPR ≥ 0.25 (shown in
 189 yellow in Figure 3c). Upon examination, we found these to have a significant river flowing right through them. Under
 190 such a scenario, the percolating heat cluster is divided structurally into two halves by a heat sink, irrespective of the
 191 threshold (Supplementary Figure 4). This results in a negative Λ_{score} due to the spacing introduced by the river despite
 192 an aggregation of heat islets on either side of the river. Thus, Figure 3c serves to quantitatively affirm the correlation
 193 between the spatial configuration of cities (dense and/or sprawling) and the 2 classes of size distributions of the heat
 194 islets.

195 Note that for any given size distribution, the islets can be spatially arranged in several ways. In order to examine
 196 the variability in islet size and spacing of the various cities, we define two scale-independent metrics to characterize
 197 size: Mean (A_M) and Largest (A_L) Relative Heat Islet Sizes, calculated as a percentage of the total city area. First,
 198 we observe that there is a weak positive correlation ($R^2 = 0.4$) between A_M and spacing of the heat-islets (Figure
 199 3d). This is expected because a positive Λ_{score} as well as a high A_M corresponds to dense cities, and a negative
 200 Λ_{score} and low A_M corresponds to sprawling cities. More noteworthy is the horizontal spread about the diagonal in
 201 Figure 3d which reflects the different spatial configurations (characterized by Λ_{score}) that are possible for any given
 202 size distribution. This spread may be explained by A_L , which increases with Λ_{score} (illustrated using marker size in
 203 Figure 3d; Supplementary Figure 5). In the bottom-left, both A_M and A_L are small. This is because negative Λ_{score}
 204 corresponds to sprawling cities where large clusters were absent in the islet-size distribution (as inferred from the
 205 exponential tempering of Pareto). In the bottom-right, however, the dominance of the largest aggregated islet results
 206 in a positive Λ_{score} despite a low A_M value. A schematic diagram drawn to represent each of the vertices of this
 207 plot is given as Supplementary Figure 6. The phase plot of A_M and Λ_{score} may be useful for city planners to gauge
 208 the current spatial structure of the thermal landscape of their cities and to determine mitigation strategies to achieve a
 209 more desirable state.

210 Islet Intensity distribution

211 Apart from the size and spacing of heat islets, we now focus on the temperatures obtained within the heat islets. To
 212 address this, we first use the well-known indicator of excess heat in urban areas, the SUHI Intensity in the traditional
 213 sense i.e., the difference between the mean urban and rural temperatures (Schwarz et al., 2011) to evaluate the average
 214 excess heat within cities. We find that larger Λ_{score} values (representative of aggregated heat islets) tend to be associ-
 215 ated with higher SUHI Intensity (Figure 4b). This suggests that sprawling cities, with a larger number of heat sinks to

216 match the heat sources, are a better configuration for reducing the *overall* SUHI Intensity. This is in agreement with our
 217 findings based on the size distribution of extreme heat islets as well as Debbage and Shephard (2015) findings based
 218 on discontinuity of urban patches calculated using National Land Cover Dataset (NLCD) (Debbage and Shepherd,
 219 2015). Traditional estimates of the UHI Intensity that simply use the difference between the **mean** temperatures over
 220 an urban area and the surrounding non-urban environment fail to address the intra-urban heterogeneity adequately.

221 For a more comprehensive assessment of the thermal variability within cities, we introduce a novel *Heat Islet*
 222 *Intensity* distribution metric. First, we compute the excess heat (ΔT) for each islet as the difference between the mean
 223 *islet* temperature and the *threshold* temperature. We refer to this term as the *Islet Intensity*. We find that the mean and
 224 standard deviation of ΔT were equal (Supplementary Figure 7) which, along with the shape of its distribution (Figure
 225 4a), were indicative that ΔT is exponentially distributed, i.e:

$$P(\Delta T \geq x) \propto 1 - e^{-\lambda x} \quad (4)$$

226 where, for a given islet intensity x , the probability of an islet having a temperature ΔT larger than x is represented
 227 by P , an exponential distribution characterized by λ . By extension, $1/\lambda$ is the mean islet intensity. Lower values of
 228 λ correspond to an increased probability of higher temperatures within the islets. Therefore, a single metric, λ can be
 229 used as an indicator to capture the intra-urban thermal variability across islets. This is represented as the color bar in
 230 Figure 4b.

231 We find that while cities with a higher degree of sprawl have a lower mean temperature, for the same SUHI (Y-axis in
 232 Figure 4b), cities with lower Λ_{score} also experience higher likelihood of encountering thermal extremes. For example,
 233 dense cities such as Lagos and Jakarta have a steeper exponential decaying rate than Chicago and Guangzhou, which
 234 drastically reduces the probability of local thermal extremes within their heat islets. While the probability of a heat
 235 islet being hotter than the mean by 1°C is almost zero for the first two, the likelihood increases to roughly 20% for the
 236 latter two (Figure 4a). As the larger heat islets are often associated with the highest islet intensity as well, this can result
 237 in a significantly large areas of extreme heat especially for megacities like Guangzhou and Chicago. Such a finding
 238 reveals that while mean SUHI Intensity decreases with sprawling cities, for the same mean, they also experience higher
 239 local thermal extremes. As a result, in addition to the mean SUHI Intensity, it is essential to characterize the thermal
 240 heterogeneity within the cities, and the islet intensity distribution can be adopted as a complementary metric.

241 **Summary and Conclusions**

242 Cities grow through a combination of parallel and sequential episodes of expansion and densification at different rates.
 243 Depending on local preferences and constraints, neighborhoods adopt different spatial patterns, for example, from
 244 dense downtowns to sprawling suburbs. Factors like geographical topography, coastline, and intra-urban commuting
 245 time constrain expansion, whereas other factors such as local building laws limit densification. While there are several
 246 objective functions such as commuting travel time distribution, net carbon emissions, and socio-economical factors
 247 which urban form and functions are optimized for, here, we focus on the aspect of urban heat. More specifically,
 248 the spatial heterogeneity of extreme heat islets within urban areas. Towards that, we present a novel multi-scale
 249 framework that allows us to identify intra-urban heat islets for several thermal thresholds. Using this framework,
 250 we evaluate the impact of spatial organization, characterized by a Lacunarity-based metric, Λ_{score} . We do not find
 251 a bi-modal distribution of Λ_{score} into two classes of sprawl or dense cities only. Rather, the Λ_{score} was normally
 252 distributed around a mean value close to zero indicating that most cities display a balance between sprawl and dense

253 heat islet structure. Different realizations and degrees of expansion and densification yield a diverse array of spatial
254 structures.

255 We condense the size, spacing, and intensity information about heterogeneous clusters into probabilistic distribu-
256 tions that can be described using single scaling exponents. This allows for a seamless comparison of the intra-urban
257 heat islet characteristics across cities at several spatial scales ranging from 90 meters (resolution of Landsat 8 and
258 corresponding to several urban blocks) up to few thousand sq km (total area of large cities). We implement this frame-
259 work for 78 globally representative cities to answer the following key questions. First, how many and how big are the
260 emergent heat islets at multiple thermal thresholds? Second, how much hotter than the threshold are these heat islets?
261 From the size distribution analysis, we demonstrate that islet sizes in dense cities follow and maintain a power law
262 tail across all temperature thresholds, whereas the sprawling cities show an exponential tempering of tails at higher
263 thresholds. Such a tempering is favourable as it indicates a reduced emergence of large heat islets in sprawling and
264 dispersed spatial configurations. Additionally, a dispersed configurations results in lower *mean SUHI Intensity* over
265 the city. However, from the islet intensity distribution analysis, we find that heat islet intensities (ΔT) can be mod-
266 elled as exponential distributions, where dispersed configurations result in higher rate parameters, λ . This implies a
267 significantly higher probability of encountering extreme temperatures within the islets. As a result, while a sprawling
268 configuration is favorable for reducing the mean temperature of a city, for the same mean SUHI intensity, it results in
269 higher local thermal extremes. Therefore, from a design decision perspective, a trade-off between mean versus local
270 thermal extremes depending on other climatological and demographic factors will be required. In cities set in hotter
271 background climates, for instance, it maybe more desirable to reduce local extremes to avoid extreme heat hazards es-
272 pecially if the local extremes occur where most vulnerable populations reside, such as densely populated downtowns,
273 or areas without access to air-conditioning such as urban slums.

274 Our analysis here is limited to the structural heterogeneity of heat sources and sinks, and not the functional hetero-
275 geneity. If we assume a uniform heat capacity of land use, the sizes of heat islets are then indicative of the strength of
276 the sources, and the length-scale of spacing is indicative of the sink strengths. Consideration of the *functional* hetero-
277 geneity will require a treatment of the variability in heat capacities and thermal conductivities of the land use which
278 jointly determine heat dissipation from sources, which is possible using models such as Weather Research Forecast
279 (WRF) (Chen et al., 2011; Salamanca et al., 2011). In such a scenario, instead of LST, heat fluxes can be treated as
280 DEM for such an analysis. It may also then be beneficial to study the spatial correlation between source strength and
281 sink strength to evaluate thermal dissipation.

282 We recognize that the spatial patterns of air temperatures (at 2 meters for example) might differ from those based on
283 SUHI derived from LST, as determined by a higher influence of atmospheric turbulence and boundary layer conditions
284 (Panwar et al., 2019). For example, a larger thermal gradient can result in turbulent eddies of larger length-scales in-
285 ducing more overturning circulation which can, in turn, reduce the temperatures in dense urban areas. An investigation
286 of the spatio-temporal dynamics of air temperatures is beyond the scope of the present study but it certainly warrants
287 further research to study the persistence of these spatial patterns. Lastly, while the spatial characterization of temper-
288 ature is informative for urban heat assessments, it does not inform the overall risk map to the concerned population.
289 Risk is a combination of hazard (extreme heat-stress, a combination of air temperature and humidity (Oleson et al.,
290 2015)), time period of exposure, and vulnerability factors such as old age, low educational attainment, high poverty
291 levels, poor health, and lack of air conditioning (Cutter et al., 2009; Uejio et al., 2011; Bradford et al., 2015). In the
292 future, we seek to characterize the spatial variability in risk through joint probability distribution analysis of each of
293 the three dimensions of risk.

294 **Methods**

295 **Study area and data sources**

296 Land surface temperature (LST) data was derived using a Single Channel Algorithm as detailed in (Walawender et al.,
 297 2012) from Landsat 8 at a resolution of 90 m. The geo-spatial analysis environment of Google Earth Engine (GEE)
 298 was used to filter out cloud free summer time days with an incident solar angle of at least 60 degrees (Gorelick et al.,
 299 2017). See Supplementary Text S1 and S2 for algorithms, and Table S1 for list of cities and information on Landsat
 300 scenes used. For coastal cities the Large Scale International Boundary (LSIB) dataset provided by United States Office
 301 of the Geographer was used to crop out the oceans and delineate urban boundaries within GEE environment. Urban
 302 area was estimated using MODIS's Land Cover Type dataset - MCD12Q1.

303 **Statistical modelling of size and intensity distributions**

304 For fitting probability distribution functions (pdfs) to cluster size and intensity distributions, a combination of
 305 maximum-likelihood estimation (mle) with goodness-of-fit tests based on the Kolmogorov-Smirnov (KS) statistic
 306 and likelihood ratios were used (Clauset et al., 2009). See Supplementary Text S3 for details and Table S2 for results.

307 **Lacunarity**

308 First, the landscape was sliced at a thermal threshold and an islets map was obtained. For each box size ($1 < r <$
 309 A_{city}), the number of occupied pixels (islets) was measured. The number of occupied sites was referred to as the
 310 box mass. The box was then moved one column to the right and the box mass was again counted. This process was
 311 repeated over all rows and columns producing a frequency distribution of the box masses. The number of boxes of size
 312 r containing S occupied sites was designated by $n(S, r)$ and the total number of boxes of size r by $N(r)$. This frequency
 313 distribution was converted into a probability distribution: $Q(S, r) = \frac{n(S, r)}{N(r)}$. Lacunarity was a measure of variability
 314 in the calculated occupancy for each box size.

$$\Lambda(r) = \frac{\text{Variance}Q(S, r)}{\text{Mean}Q(S, r)^2} + 1 \quad (5)$$

315 For all cities, Lacunarity score was calculated only for the 90th percentile thermal threshold. As a result, 90% of the
 316 total area in all cases comprised of spaces and the $\Lambda(r)$ value for box size = 1 was the same for all cities. The largest
 317 box size taken under consideration is normalized from 0 to 100 in order to account for the variable sizes of cities. Note
 318 that the curvature of Lacunarity curve was unaffected by these transformations.

319 **Acknowledgments**

320 The authors thank the organizers and participants of a series of Complex Networks Synthesis workshops; co-hosted
 321 by Purdue University, University of Florida, Helmholtz Centre for Environmental Research, UFZ, and Technical Uni-
 322 versity, Dresden, Germany; for creating a trans-disciplinary collaborative research environment and providing critical
 323 input across multiple workshops. The authors appreciate the discussions on lacunarity with Prof. Joaquín C. Goñi.
 324 A.S. and S.B. gratefully acknowledge the financial support from NASA in the form of their NASA Earth and Space
 325 Science Fellowships (Grant numbers: 80NSSC17K0441 and NNX15AM72H, respectively). P.S.C.R. acknowledges

326 the support from NSF Collaborative Research - RIPS Type 2: Resilience Simulation for Water, Power and Road
 327 Networks (1441188) and the Lee A. Reith Endowment in the Lyles School of Civil Engineering at Purdue University.

328 **References**

- 329 Amaral, L. A. N., A. Scala, M. Barthelemy, and H. E. Stanley, 2000: Classes of small-world networks. *Proceedings of*
 330 *the national academy of sciences*, **97 (21)**, 11 149–11 152.
- 331 Andersson, C., K. Frenken, and A. Hellervik, 2006: A complex network approach to urban growth. *Environment and*
 332 *Planning A*, **38 (10)**, 1941–1964.
- 333 Andreou, E., 2013: Thermal comfort in outdoor spaces and urban canyon microclimate. *Renewable Energy*, **55**, 182–
 334 188.
- 335 Barabási, A.-L., and R. Albert, 1999: Emergence of scaling in random networks. *science*, **286 (5439)**, 509–512.
- 336 Barthelemy, M., 2016: *The structure and dynamics of cities*. Cambridge University Press.
- 337 Batty, M., 2008: The size, scale, and shape of cities. *science*, **319 (5864)**, 769–771.
- 338 Batty, M., 2013: *The new science of cities*. Mit Press.
- 339 Bradford, K., L. Abrahams, M. Hegglin, and K. Klima, 2015: A heat vulnerability index and adaptation solutions for
 340 pittsburgh, pennsylvania. *Environmental Science & Technology*, **49 (19)**, 11 303–11 311.
- 341 Chen, F., and Coauthors, 2011: The integrated wrf/urban modelling system: development, evaluation, and applications
 342 to urban environmental problems. *International Journal of Climatology*, **31 (2)**, 273–288.
- 343 Ching, J., and Coauthors, 2018: Wudapt: An urban weather, climate, and environmental modeling infrastructure for
 344 the anthropocene. *Bulletin of the American Meteorological Society*, **99 (9)**, 1907–1924.
- 345 Clauset, A., C. R. Shalizi, and M. E. Newman, 2009: Power-law distributions in empirical data. *SIAM Review*, **51 (4)**,
 346 661–703.
- 347 Cottineau, C., E. Hatna, E. Arcaute, and M. Batty, 2017: Diverse cities or the systematic paradox of urban scaling
 348 laws. *Computers, environment and urban systems*, **63**, 80–94.
- 349 Cutter, S. L., C. T. Emrich, J. J. Webb, and D. Morath, 2009: Social vulnerability to climate variability hazards: A
 350 review of the literature. *Final Report to Oxfam America*, **5**, 1–44.
- 351 Debbage, N., and J. M. Shepherd, 2015: The urban heat island effect and city contiguity. *Computers, Environment and*
 352 *Urban Systems*, **54**, 181–194.
- 353 Gorelick, N., M. Hancher, M. Dixon, S. Ilyushchenko, D. Thau, and R. Moore, 2017: Google earth engine: Planetary-
 354 scale geospatial analysis for everyone. *Remote Sensing of Environment*, **202**, 18–27.
- 355 Imre, A. R., and J. Novotný, 2016: Fractals and the korcak-law: a history and a correction. *The European Physical*
 356 *Journal H*, **41 (1)**, 69–91.
- 357 Isichenko, M., and J. Kalda, 1991: Statistical topography. i. fractal dimension of coastlines and number-area rule for
 358 islands. *Journal of Nonlinear Science*, **1 (3)**, 255–277.
- 359 Isichenko, M. B., 1992: Percolation, statistical topography, and transport in random media. *Reviews of Modern*
 360 *Physics*, **64 (4)**, 961.
- 361 Jamei, E., P. Rajagopalan, M. Seyedmahmoudian, and Y. Jamei, 2016: Review on the impact of urban geometry and
 362 pedestrian level greening on outdoor thermal comfort. *Renewable and Sustainable Energy Reviews*, **54**, 1002–1017.
- 363 Klinkhamer, C., E. Krueger, X. Zhan, F. Blumensaat, S. Ukkusuri, and P. S. C. Rao, 2017: Functionally fractal urban
 364 networks: Geospatial co-location and homogeneity of infrastructure. *arXiv preprint arXiv:1712.03883*.

- 365 Li, D., and E. Bou-Zeid, 2013: Synergistic interactions between urban heat islands and heat waves: the impact in cities
366 is larger than the sum of its parts. *Journal of Applied Meteorology and Climatology*, **52** (9), 2051–2064.
- 367 Mandelbrot, B. B., 1975: Stochastic models for the earth’s relief, the shape and the fractal dimension of the coastlines,
368 and the number-area rule for islands. *Proceedings of the National Academy of Sciences*, **72** (10), 3825–3828.
- 369 Mandelbrot, B. B., 1982: *The fractal geometry of nature*, Vol. 2. WH freeman New York.
- 370 Mohajeri, N., A. Gudmundsson, and J.-L. Scartezzini, 2015: Expansion and densification of cities: linking urban form
371 to ecology. *Proceedings of International Conference CISBAT 2015 Future Buildings and Districts Sustainability*
372 *from Nano to Urban Scale*, LESO-PB, EPFL, 475–480, CONF.
- 373 Mustafa, A., A. Heppenstall, H. Omrani, I. Saadi, M. Cools, and J. Teller, 2018: Modelling built-up expansion and
374 densification with multinomial logistic regression, cellular automata and genetic algorithm. *Computers, Environ-*
375 *ment and Urban Systems*, **67**, 147–156.
- 376 Nikolopoulou, M., and S. Lykoudis, 2006: Thermal comfort in outdoor urban spaces: analysis across different euro-
377 pean countries. *Building and environment*, **41** (11), 1455–1470.
- 378 Oleson, K., A. Monaghan, O. Wilhelmi, M. Barlage, N. Brunzell, J. Feddema, L. Hu, and D. Steinhoff, 2015: Interac-
379 tions between urbanization, heat stress, and climate change. *Climatic Change*, **129** (3-4), 525–541.
- 380 Panwar, A., A. Kleidon, and M. Renner, 2019: Do surface and air temperatures contain similar imprints of evaporative
381 conditions? *Geophysical Research Letters*.
- 382 Peel, M. C., B. L. Finlayson, and T. A. McMahon, 2007: Updated world map of the köppen-geiger climate classifica-
383 tion. *Hydrology and Earth System Sciences*, **4** (2), 439–473.
- 384 Plotnick, R. E., R. H. Gardner, W. W. Hargrove, K. Prestegaard, and M. Perlmutter, 1996: Lacunarity analysis: a
385 general technique for the analysis of spatial patterns. *Physical review E*, **53** (5), 5461.
- 386 Plotnick, R. E., R. H. Gardner, and R. V. O’Neill, 1993: Lacunarity indices as measures of landscape texture. *Land-*
387 *scape ecology*, **8** (3), 201–211.
- 388 Prudhomme, M., 2018: World urbanization prospects: The 2018 revision. *UN Department of Public Information*,
389 available online: [https://www.un.org/development/desa/en/news/population/2018-revision-of-world-urbanization-](https://www.un.org/development/desa/en/news/population/2018-revision-of-world-urbanization-prospects.html)
390 [prospects.html](https://www.un.org/development/desa/en/news/population/2018-revision-of-world-urbanization-prospects.html).
- 391 Rotach, M., and Coauthors, 2005: Bubble—an urban boundary layer meteorology project. *Theoretical and Applied*
392 *Climatology*, **81** (3-4), 231–261.
- 393 Roth, M., T. Oke, and W. Emery, 1989: Satellite-derived urban heat islands from three coastal cities and the utilization
394 of such data in urban climatology. *International Journal of Remote Sensing*, **10** (11), 1699–1720.
- 395 Sahimi, M., and M. Sahimi, 2014: *Applications of percolation theory*. CRC Press.
- 396 Salamanca, F., A. Martilli, M. Tewari, and F. Chen, 2011: A study of the urban boundary layer using different ur-
397 ban parameterizations and high-resolution urban canopy parameters with wrf. *Journal of Applied Meteorology and*
398 *Climatology*, **50** (5), 1107–1128.
- 399 Santamouris, M., 2014: On the energy impact of urban heat island and global warming on buildings. *Energy and*
400 *Buildings*, **82**, 100–113.
- 401 Schwarz, N., S. Lautenbach, and R. Seppelt, 2011: Exploring indicators for quantifying surface urban heat islands of
402 european cities with modis land surface temperatures. *Remote Sensing of Environment*, **115** (12), 3175–3186.
- 403 Schwarz, N., and A. M. Manceur, 2014: Analyzing the influence of urban forms on surface urban heat islands in
404 europe. *Journal of Urban Planning and Development*, **141** (3), A4014003.

- 405 Semenza, J. C., C. H. Rubin, K. H. Falter, J. D. Selanikio, W. D. Flanders, H. L. Howe, and J. L. Wilhelm, 1996:
406 Heat-related deaths during the July 1995 heat wave in Chicago. *New England Journal of Medicine*, **335** (2), 84–90.
- 407 Seto, K. C., and J. M. Shepherd, 2009: Global urban land-use trends and climate impacts. *Current Opinion in Envi-*
408 *ronmental Sustainability*, **1** (1), 89–95.
- 409 Shreevastava, A., P. S. C. Rao, and G. McGrath, 2019: Emergent scaling of intra-urban heat islets across global cities.
410 *Submitted to Physical Reviews E*.
- 411 Shreevastava, A., P. S. C. Rao, and G. S. McGrath, 2018: Spatial analysis of the surface urban heat island. *Land*
412 *Surface and Cryosphere Remote Sensing IV*, International Society for Optics and Photonics, Vol. 10777, 107770C.
- 413 Sobstyl, J., T. Emig, M. A. Qomi, F.-J. Ulm, and R.-M. Pellenq, 2018: Role of city texture in urban heat islands at
414 nighttime. *Physical review letters*, **120** (10), 108 701.
- 415 Stewart, I. D., and T. R. Oke, 2012: Local climate zones for urban temperature studies. *Bulletin of the American*
416 *Meteorological Society*, **93** (12), 1879–1900.
- 417 Stone, B., J. J. Hess, and H. Frumkin, 2010: Urban form and extreme heat events: are sprawling cities more vulnerable
418 to climate change than compact cities? *Environmental health perspectives*, **118** (10), 1425.
- 419 Stone Jr, B., and M. O. Rodgers, 2001: Urban form and thermal efficiency: how the design of cities influences the
420 urban heat island effect. *American Planning Association. Journal of the American Planning Association*, **67** (2),
421 186.
- 422 Taleghani, M., L. Kleerekoper, M. Tenpierik, and A. van den Dobbelsteen, 2015: Outdoor thermal comfort within five
423 different urban forms in the Netherlands. *Building and environment*, **83**, 65–78.
- 424 Uejio, C. K., O. V. Wilhelmi, J. S. Golden, D. M. Mills, S. P. Gulino, and J. P. Samenow, 2011: Intra-urban societal vul-
425 nerability to extreme heat: the role of heat exposure and the built environment, socioeconomics, and neighborhood
426 stability. *Health & Place*, **17** (2), 498–507.
- 427 Voogt, J. A., and T. R. Oke, 2003: Thermal remote sensing of urban climates. *Remote Sensing of Environment*, **86** (3),
428 370–384.
- 429 Walawender, J. P., M. J. Hajto, and P. Iwaniuk, 2012: A new ArcGIS toolset for automated mapping of land surface
430 temperature with the use of Landsat satellite data. *Geoscience and Remote Sensing Symposium (IGARSS), 2012 IEEE*
431 *International*, IEEE, 4371–4374.
- 432 Yang, S., K. Paik, G. S. McGrath, C. Urich, E. Krueger, P. Kumar, and P. S. C. Rao, 2017: Functional topology of
433 evolving urban drainage networks. *Water Resources Research*, **53** (11), 8966–8979.
- 434 Zhao, L., X. Lee, R. B. Smith, and K. Oleson, 2014: Strong contributions of local background climate to urban heat
435 islands. *Nature*, **511** (7508), 216.
- 436 Zhao, L., M. Oppenheimer, Q. Zhu, J. W. Baldwin, K. L. Ebi, E. Bou-Zeid, K. Guan, and X. Liu, 2018: Interactions
437 between urban heat islands and heat waves. *Environmental research letters*, **13** (3), 034 003.

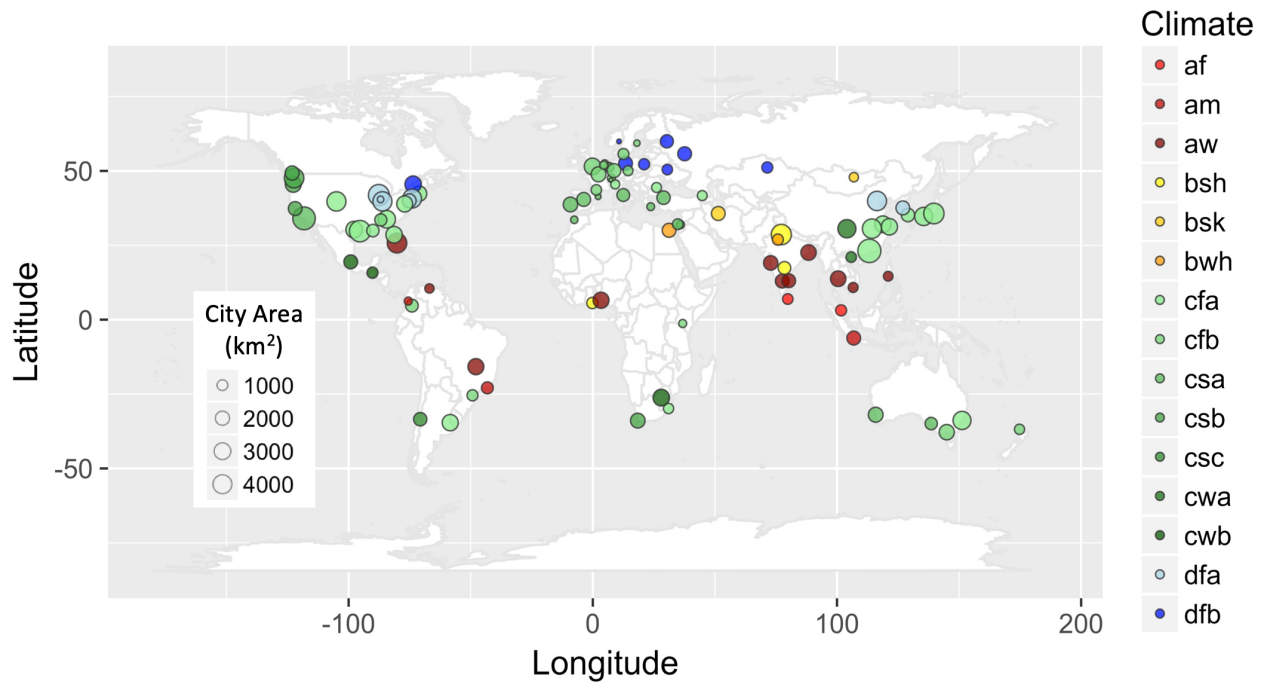
438 **Figures**

Figure 1: World map showing the locations of 78 cities considered in this study. The marker size is representative of the city size, and the colour represents their Koppen-Geiger climate classification Peel et al. (2007). Description of Koppen-Geiger climate types are given in Supplementary Table 1.

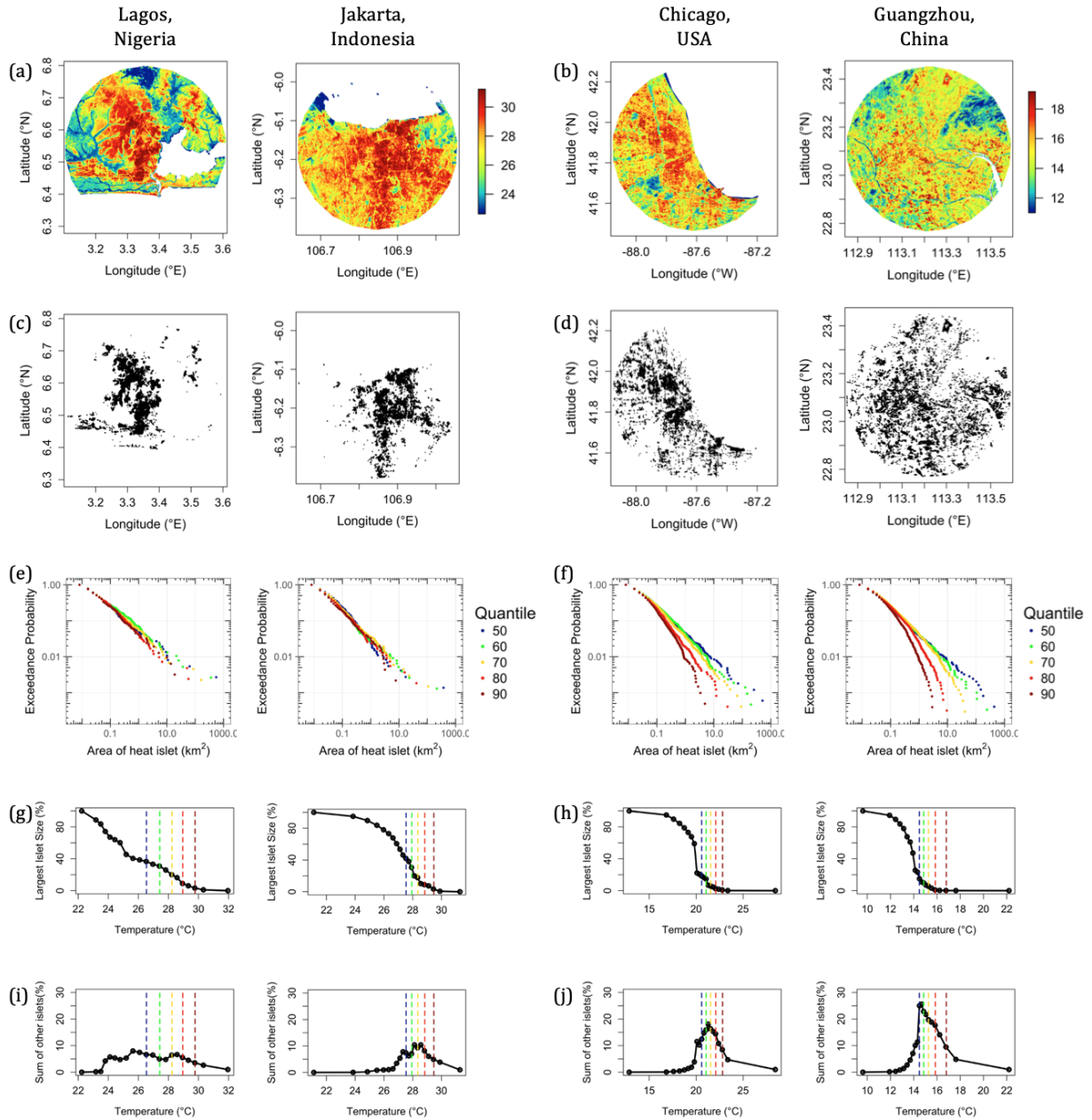


Figure 2: Two groups of cities emerge based on the size distributions of heat islets at incremental thermal thresholds. Two representative cities for each group - Jakarta, Indonesia and Lagos, Nigeria for dense cities, and Chicago, USA, and Guangzhou, China for sprawling cities - are shown. (a,b) Land Surface Temperature map (in $^{\circ}\text{C}$), (c,d) Heat islets that emerge at the 90th percentile thermal threshold, (e,f) Exceedance probability plots for heat islets at several thermal thresholds (50th, \dots , 90th). Note the leftward shift in size distribution as the thresholds increase, especially the exponential tempering evident in sprawling cities, (g,h) Largest islet size, and (i,j) sum of remaining islets (as a % of total city area), as a function of thermal threshold. The vertical dashed coloured lines mark the temperatures corresponding to the percentiles used in (e,f).

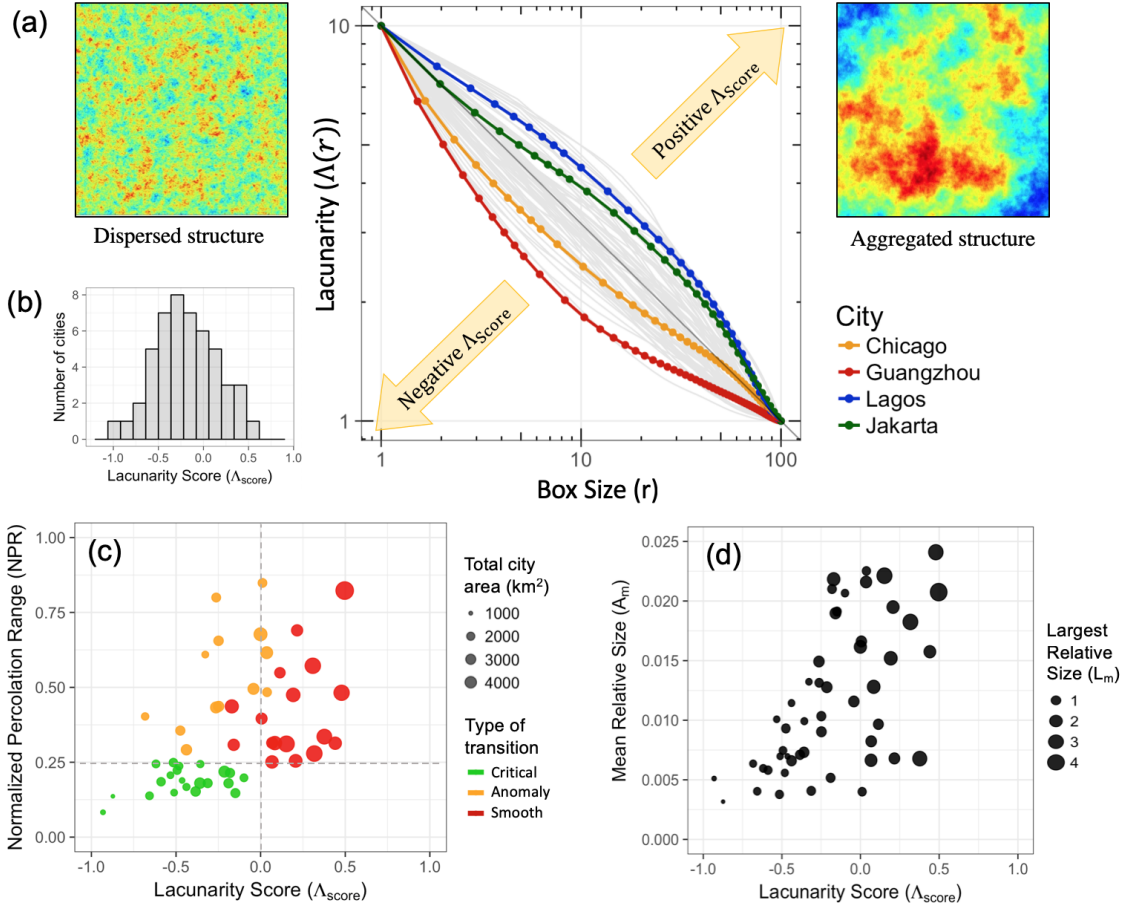


Figure 3: (a) Lacunarity curves of 49 cities (in grey) and the four archetype cities (in colour) shown on a $\log(\Lambda)$ vs $\log(r)$ plot. The cities with a concave downwards shape in the upper side of the diagonal indicate larger and more aggregated gaps, whereas cities underneath the curve indicate a more uniform dispersed pattern of islets and smaller gaps. (b) Histogram of Λ_{score} of 49 cities (mean = 0.04, s.d. = 0.38). (c) Scatter plot of percolation transition range and Lacunarity score. This figure illustrates the classification of cities into the 2 classes based on Lacunarity Score and the type of transition. (d) Scatter plot of Mean Relative Heat Islet Size (A_M) versus Λ_{score} . Additionally, since the islet-size distribution is heavy tailed, in addition to the A_M , the largest islet size (as a percentage of the total city area) is indicated using the marker size. The A_M and the largest-heat islet size (A_L) serve to illustrate the size distribution of the hottest islets occupying the ten percent of the city area.

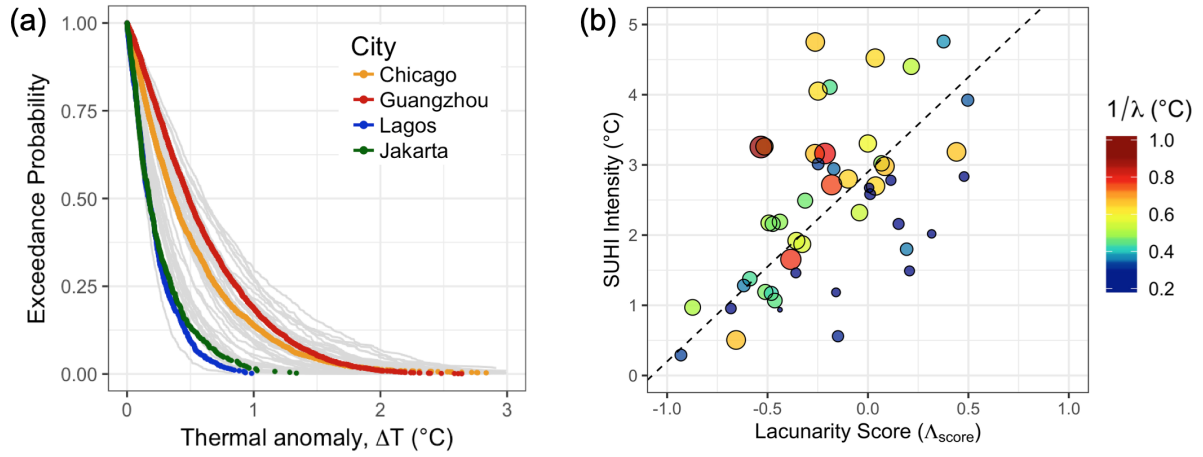


Figure 4: (a) Empirical pdf of ΔT for the 4 archetype cities shown on at their 90th percentile thermal thresholds respectively. The same for all 49 cities is shown in grey in the background. Each ΔT distribution was well described as an exponential distribution characterized by the parameter: λ . (b) Scatter plot of mean SUHI Intensity, defined as the difference between mean urban and rural temperatures, versus Lacunarity Score (Λ_{score}) is shown. A weak positive correlation ($R^2 = 0.344$) is detected shown as dashed regression line. The color as well as size of the marker indicates the inverse of rate parameter (λ) from Equation 4 which is equal to the mean Heat Islet Intensity for each distribution. Increasing size indicates higher temperatures within the heat islets.